



Effects of inter-organism interactions in biofouling on microtopographic surfaces

Trinh X. Hoang, Ha T. H. Mai, Anthony B. Brennan & Ly Le


To cite this article: Trinh X. Hoang, Ha T. H. Mai, Anthony B. Brennan & Ly Le (2019) Effects of inter-organism interactions in biofouling on microtopographic surfaces, *Biofouling*, 35:6, 684-695, DOI: [10.1080/08927014.2019.1650918](https://doi.org/10.1080/08927014.2019.1650918)

To link to this article: <https://doi.org/10.1080/08927014.2019.1650918>



Published online: 20 Aug 2019.



[Submit your article to this journal](#) 



Article views: 44



[View related articles](#) 



[View Crossmark data](#) 



Effects of inter-organism interactions in biofouling on microtopographic surfaces

Trinh X. Hoang^{a,b}, Ha T. H. Mai^c, Anthony B. Brennan^d and Ly Le^e

^aInstitute of Physics, Vietnam Academy of Science and Technology, Ba Dinh, Ha Noi, Vietnam; ^bPhysics Department, Graduate University of Science and Technology, Vietnam Academy of Science and Technology, Cau Giay, Ha Noi, Vietnam; ^cInstitute for Environmental and Transport Studies, Ho Chi Minh City University of Transport, Ho Chi Minh City, Vietnam; ^dDepartment of Materials Science and Engineering, University of Florida, Gainesville, FL, USA; ^eSchool of Biotechnology, International University, Vietnam National University, Ho Chi Minh City, Vietnam

ABSTRACT

An extended model of the surface energetic attachment (SEA) model is introduced to study the fouling of marine organisms on microtopographic surfaces, taking into account the excluded volume interaction and the attraction between the organisms. It is shown that the excluded volume interaction leads to changes in the site-typed attachment probabilities which increase with the average spore density on the surface. As a result of these changes, the spore density map is flattened under very high density fouling. The attractive interaction on the other hand leads to aggregation of spores and the average aggregate size increased with the strength of attraction. The model can be mapped to a specific experiment to determine the attachment energy parameters. In contrast to various prior empirical approaches, the extended SEA model is rigorous from the statistical mechanics viewpoint, thus it provides a reliable tool for studying complex attachment behaviors of microorganisms on topographic surfaces.

ARTICLE HISTORY

Received 5 April 2019
Accepted 29 July 2019

KEYWORDS

Sharklet; attachment model; excluded volume; Monte Carlo simulation; *Ulva*; high-density fouling; aggregation

Introduction

Recently, there has been much attention to engineered microtopographic surfaces as potential nontoxic anti-fouling (AF) strategies to replace the use of toxic paints in the marine environment, particularly on ships' hulls (Carman et al. 2006; Magin, Cooper, et al. 2010; Thomas and Brooks 2010; Scardino and de Nys 2011; Kirschner and Brennan 2012). Studies have shown that certain types of surface topography can reduce the attachment of marine microorganisms, such as *Ulva*, as much as 77% compared to a smooth surface (Schumacher, Aldred, et al. 2007). The AF effectiveness of microtopographic surfaces however depends strongly and variably on their topographic characteristics, such as feature configuration (Efimenko et al. 2009), feature shape (Schumacher, Carman, et al. 2007), size and aspect ratio (Schumacher, Aldred, et al. 2007), by a mechanism that is still far from being well understood (Bloecher et al. 2013). Several theoretical models have been developed to predict attachment behaviors of marine organisms on topographic surfaces.

One of the earliest models proposed was the attachment point theory (APT) (Callow et al. 2002;

Scardino et al. 2006, 2008), which was based on the observation that marine organisms preferentially bind to locations where they can maximize the number of contact points with a surface. This theory received only a partial support from experiments. It has been shown that the number of attachment points alone is insufficient to predict the relative changes in fouling for different organisms on a given topography (Scardino et al. 2008). More importantly, the attachment point theory does not provide a way to calculate the relative attachment density of organisms on topographies in which the numbers of attachment points differ in different locations.

Another model that has shown limited success is the engineered roughness index (ERI) (Long, Finlay, et al. 2010). The ERI model was derived from the theories of wetting of a textured surface and considers the topographic properties of the surface such as the Wenzel roughness (Wenzel 1936), the number of distinct features and the fractional area of feature tops as defined by the Cassie–Baxter theory (Cassie and Baxter 1944). It related the relative attachment density of organisms to the calculated engineered roughness index through a logarithmic dependence with an

experimentally fitted slope. Amendments to the ERI model include adding the Reynold's number of an organism to account for the impact of the size and shape of the organism on fouling (Magin, Long, et al. 2010; Magin et al. 2011). The ERI model predicts the relative settlement of organisms quite well but only for the cases of AF, ie decreases in the fouling density. The model fails to quantify the changes when there are increases in the density of the organisms on a topographic surface compared to an unpatterned surface (Xiao et al. 2013).

The surface energetic attachment (SEA) model (Decker et al. 2013) was developed in an attempt to include fouling on microtopographies for which both the increase and the decrease in fouling density were described. In contrast to the empirical basis of the previous APT and ERI models, the SEA model was derived based on the principles of statistical mechanics. The model explicitly considers the surface topography with an appropriate discretization on a lattice. An attachment energy was assigned to the binding of an organism to the surface. This energy was proposed to depend linearly on the contact area between the organism and the surface. In the simplest approximation, it may be assumed that the attachment energy was only proportional to the number of attachment points. The relative attachment density of organisms was then calculated using a probability of attachment based upon the Boltzmann distribution for a fixed temperature.

The SEA model has shown a good regression to experimental data of attachment density for a variety of organisms on different surface topographies (Decker et al. 2013). The model was also shown to cover two different regimes of fouling: the so-called "Wenzel wetting state" (Marmur 2003), in which the organism can settle between features and effectively "wets" all of the available areas, and the "Cassie wetting state", in which only the tops of the features are "wetted" by the organism.

From the statistical mechanics point of view, the SEA model was effectively a single organism model, ie it did not address the interactions between multiple organisms. Thus, this model worked well in the case of a very low attachment density with minimal aggregation of organisms. It can be expected that the inter-organism interactions would play an important role in the high-density fouling, both locally and globally. On a locally high-density fouling surface, organisms can attach individually or form high-density aggregates in which the average density, of the total, exposed surface, remains low. Whereas, with attachment on a globally high-density fouling surface, the density of organisms

in the aggregates would still be high but the average density will be high also. The individual fouling condition on surfaces, as well as the progression from low to high densities, can be monitored by fluorescence microscope as well as scanning electron microscopy (Long, Finlay, et al. 2010).

A basic interaction in a multiple organism system is excluded volume, which is due to the physical size of each organism. As a result of excluded volume, two organisms cannot occupy the same site on a surface nor at a distance smaller than their physical diameter. Apart from excluded volume, the effective interaction between two nearby organisms can be either repulsive or attractive when they are in physical contact with each other. This repulsion/attraction may arise due to physico-chemical properties of macromolecules on the surfaces of the organisms and/or to hydrophobic and hydrodynamic effects. For example, the specific recognition and binding of a cell-surface-associated protein adhesin to a complementary cell-surface-associated polysaccharide receptor are responsible for bacterial aggregation in biofilms (Schembri et al. 2003; Katharios-Lanwermeier et al. 2014). Hydrophobicity as well as electrostatic charges of the cell surface affect not only the binding affinity of organisms to a surface but also their autoaggregation (Del Re et al. 2000). It has been reported that hydrodynamic shear rates can monitor the relative proportion of autoaggregating and coaggregating species in freshwater biofilms (Rickard et al. 2004). A common tendency of microorganisms is to exist as social communities. Free-swimming zoospores may exhibit mutual attraction and autoaggregation due to chemotaxis, which is based on the extracellular small-molecule signaling and response mechanisms of microorganisms (Thomas and Peterson 1990; Reid et al. 1995; Savory et al. 2014).

The purpose of this study was to investigate the effects of excluded volume and attractive interactions on the fouling behaviors of organisms attaching to a surface at low to high densities. To perform this task, the SEA model was extended to describe systems of multiple interacting spores on a topographic lattice and Monte Carlo simulations were carried out to study their equilibrium properties. The results for interacting spores are compared to those of non-interacting spores.

Materials and methods

SEA model for non-interacting spores

For convenience the fouling organisms are referred to as spores of spherical shape with a diameter $d = 5 \mu\text{m}$.

Consider a system of N spores residing on a topographic surface of a given size. The surface is mapped onto a 2-D lattice, such that the spores can have only positions centered on the lattice sites. As a result of the surface topography, the lattice sites are divided into several types of different attachment properties, such as of different numbers of attachment points. A spore is given an attachment energy E_t if it attaches to the site of type t , ie topography. Let N_t be the number of spores attached to the sites of type t . The following is obtained:

$$N = \sum_t N_t, \quad (1)$$

where the summation is taken over all possible values of t . The SEA model (Decker et al. 2013) postulates that the spore configurations on the lattice are in a thermodynamic equilibrium at some temperature T , ie they form a canonical ensemble. The probability of spore attachment to site type t is given according to the Boltzmann distribution:

$$p_t = \frac{\langle N_t \rangle}{N} = \frac{g_t e^{-E_t/kT}}{Z}, \quad (2)$$

where k is the Boltzmann constant, g_t is the number of sites of type t on the lattice, $\langle N_t \rangle$ is the average number of spores on sites of type t , and Z is the partition function given by:

$$Z = \sum_t g_t e^{-E_t/kT}. \quad (3)$$

Note that the probability in Equation 2 is independent from N , meaning that the spore–spore interactions are ignored. Thus, the system of N spores is always equivalent to the system of 1 spore in terms of site-typed attachment probabilities.

From Equation 2, it follows that for any pair of site types t and u of the same surface:

$$\log \left(\frac{p_t}{p_u} \right) = \log \left(\frac{g_t}{g_u} \right) - \frac{E_t - E_u}{kT}. \quad (4)$$

Equation 4 indicates that the attachment probabilities depend only on the energy difference between different site types.

Consider now a planar smooth surface of an arbitrary material where all the lattice sites are of the same type s (for ‘smooth’) and to each site an attached spore has an energy E_s . If the same fouling condition is applied to the smooth surface as to the topographic surface, then the spore attachment probability on the smooth surface also follows the Boltzmann distribution, leading to the following equation:

$$\frac{N_s}{N} = \frac{g_s e^{-E_s/kT}}{Z}, \quad (5)$$

where N_s is the number of spores attached to the smooth surface and g_s is the number of lattice sites of type s . For any pair of lattice site types t and s , it follows from Equations 2 and 5 that:

$$\log \left(\frac{N_t}{N_s} \right) = \log \left(\frac{g_t}{g_s} \right) - \frac{(E_t - E_s)}{kT}. \quad (6)$$

Equation 6 can be used to relate attachment numbers on various topographies.

The smooth surface as introduced above plays the role of a reference surface for checking the validity of the SEA model. For given N_s and g_s , the energy parameter E_s can be calculated from Equation 5 as:

$$E_s = -kT \log \left(\frac{ZN_s}{Ng_s} \right). \quad (7)$$

In the present study, for convenience, the smooth surface was assumed to have the same size as the topographic surface, ie:

$$g_s = \sum_{t=1}^3 g_t, \quad (8)$$

whereas N_s can be an arbitrary positive number.

SEA model for interacting spores

An extended SEA model is proposed to describe a system of N interacting spores. Simple pairwise interactions for the spores are considered. First, all spores are subject to excluded volume interaction, that is the distance between any two spores must not be smaller than the diameter d of a spore. Second, neighboring spores may have a short-range attraction or repulsion to each other. Specifically, an energy E_{int} is given to a contact between two spores if their center-to-center distance is smaller than a cutoff distance of $R_c = 6 \mu\text{m}$. The contact is favorable if $E_{\text{int}} < 0$ and unfavorable if $E_{\text{int}} > 0$. If $E_{\text{int}} = 0$, only the excluded volume interaction exists.

The energy of a given spore configuration Γ on the lattice is given by:

$$E(\Gamma) = \sum_t N_t E_t + N_{\text{int}} E_{\text{int}}, \quad (9)$$

where N_{int} is the number of spore–spore contacts in the system. In the canonical ensemble, the probability of observing the configuration Γ is given by:

$$p(\Gamma) = \frac{e^{-E(\Gamma)/kT}}{Z_N} \text{ with } Z_N = \sum_{\Gamma} e^{-E(\Gamma)/kT}, \quad (10)$$

where the summation is taken over all possible configurations on the lattice. The average number of spores attached to the sites of a given type is now given by:

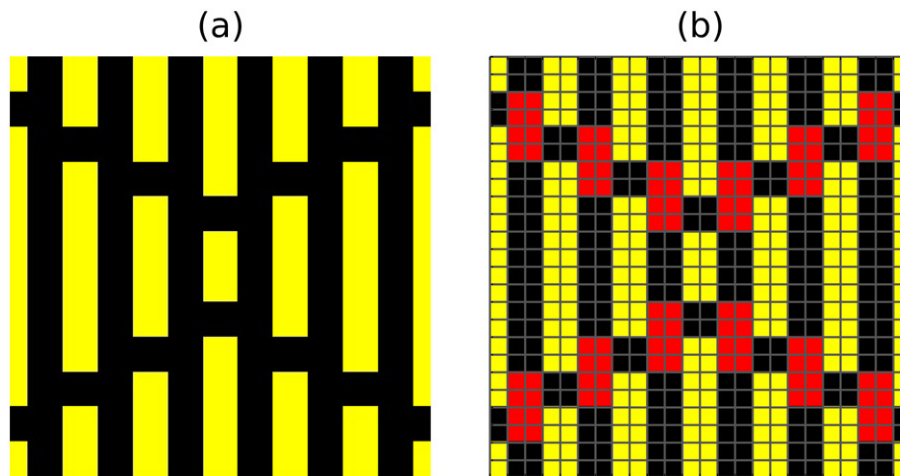


Figure 1. (a) A Sharklet unit cell with four distinct features (yellow). The feature width and the feature spacing are equal to $2\ \mu\text{m}$. The feature lengths are 4, 8, 12, and $16\ \mu\text{m}$. The size of the unit cell is $24\ \mu\text{m} \times 24\ \mu\text{m}$. (b) Discretization of the unit cell shown in (a) on a square lattice with the lattice spacing equal to $1\ \mu\text{m}$. The lattice sites are shown with colors according to their site type t , specifically $t=1$ (yellow), $t=2$ (black) and $t=3$ (red). The site type corresponds to the number of attachment points a spore can make with the surface at that site.

$$\langle N_t \rangle = \sum_{\Gamma} N_t(\Gamma) p(\Gamma). \quad (11)$$

The average in Equation 11 can be calculated by using the Monte Carlo simulation method.

Surface topography

The Sharklet topography as shown in Figure 1a was considered, in which the feature width and feature spacing were fixed and equal to $2\ \mu\text{m}$, whereas the feature lengths and the number of distinct features can be varied. Following Decker et al. (2013), the topography was discretized on a square lattice with the lattice spacing equal to $1\ \mu\text{m}$ as shown in Figure 1b. Thus, each feature width and feature spacing corresponds to two lattice constants. A lattice site is of one of three types, denoted by $t=1, 2$, and 3 , depending on the number of attachment points a spore can make with it. The sites of $t=1$ type belong to the feature tops and have only one attachment point. The sites of $t=2$ type provide two attachment points and are in the depressed spaces between features except at positions near the corners of the features. The type $t=3$ sites are between the feature corners and enable three attachment points with the spore. Surface dimensions that are multiple repeats of a rectangular unit cell were considered. Periodic boundary conditions were applied for the spores in both x and y directions of the surface plane.

Monte Carlo simulation

Monte Carlo simulations were carried out for the systems of interacting spores. The sampling of the spore

configuration space was done by employing local moves on the lattice. At the beginning of a simulation, a random configuration of spores on the lattice was generated such that the spores do not overlap with each other. At each simulation step, an attempt was made to move a randomly chosen spore to a randomly chosen neighboring lattice site. The move was rejected if it violated the excluded volume constraint, otherwise it was accepted according to the Metropolis algorithm (Metropolis et al. 1953). Specifically, for each move the energy change associated with the move $\Delta E = E_{\text{new}} - E_{\text{old}}$ is calculated. The move is always accepted if $\Delta E \leq 0$, otherwise it is accepted with the probability $p = \exp(-\Delta E/kT)$. The simulations were first run for some time, typically of the order of 10^6 steps, to equilibrate the systems. The spore attachment properties then were calculated as averages over spore configurations taken from the simulations after equilibration.

Results and discussion

Effects of excluded volume interaction

First, the effects of excluded volume interaction on the spore attachment densities were considered. For a qualitative assessment of these effects and without referring to a particular experiment, the attachment energies were taken to be $E_1 = -1\ kT$, $E_2 = -2\ kT$, and $E_3 = -3\ kT$ for the three site types. Note that these chosen energy parameters are proportional to the numbers of attachment points of the site types. Monte Carlo simulations were carried out for the

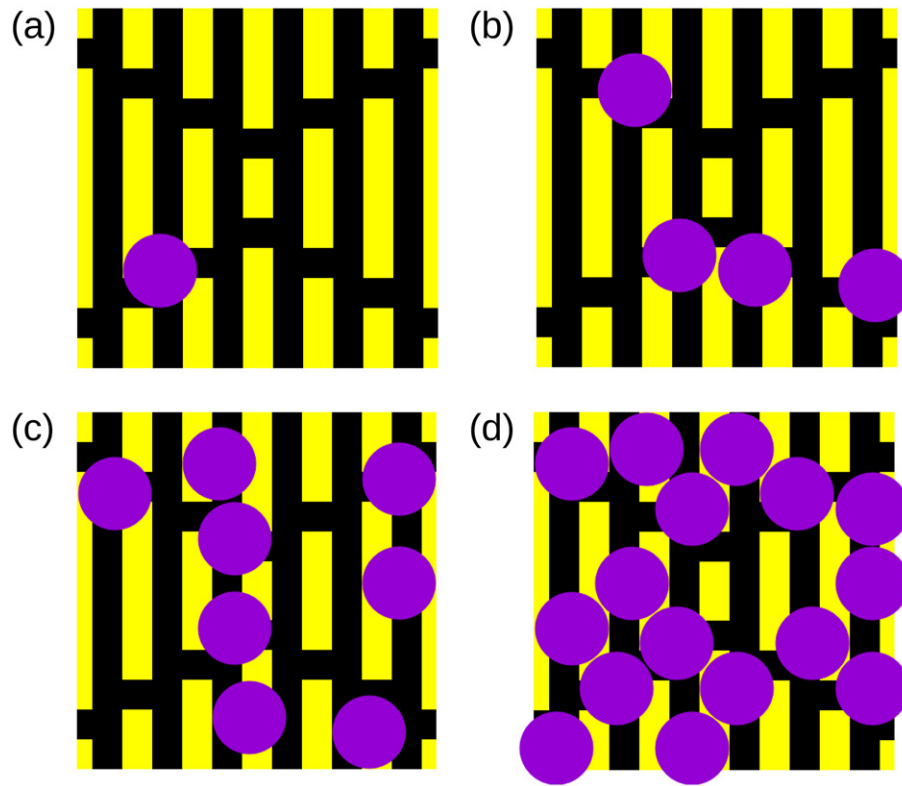


Figure 2. Examples of spore configuration for $N=1$ (a), $N=4$ (b), $N=8$ (c) and $N=16$ (d) on a single Sharklet unit cell. The spores are of diameter $d=5\ \mu\text{m}$ and shown as filled circles. The configurations shown are equilibrium configurations obtained in Monte Carlo simulations for systems with only excluded volume interaction and with attachment energy parameters $E_1 = -1\ kT$, $E_2 = -2\ kT$, and $E_3 = -3\ kT$.

fouling of N spores on a single four-featured Sharklet unit cell with N varied between 1 and 16.

Figure 2 illustrates the equilibrium configurations for various numbers of spores on the unit cell. The cases of $N=1$ and $N=4$, corresponding to low and medium average densities of spores, revealed that all the spores attached to the sites of $t=3$ near the feature corners to maximize their number of attachment points with the surface. For the cases of $N=8$ and $N=16$, corresponding to high and very high average densities, some spores did not attach to the $t=3$ sites. This was due to the fact that access to the most preferential attachment sites of these spores was hindered by other spores.

Figure 3 shows the attachment density maps, for the systems considered in Figure 2, where it is observed that the highest attachment densities correspond to the $t=3$ sites and the lowest correspond to the $t=1$ sites. The relative differences between the attachment densities for different site types, however, decreased as the number of spores increased. Especially, for the case of $N=16$, the densities at $t=3$ sites are almost indistinguishable from those at $t=2$ sites, except at very few spots. Note that the system of non-interacting spores corresponds to $N=1$

case, thus the effect of excluded volume interaction is clearly seen on the density maps.

Figure 4a shows that the site-typed attachment probability (N_t/N) depends on N differently for different site types, specifically, the attachment probability for $t=3$ sites decreases with N while those of $t=1$ and $t=2$ sites increases. These dependencies on N are almost linear for all three site types. Figure 4b shows the dependence of the site-typed average occupation number, the number of spores per lattice site (N_t/g_t), on the total number of spores N for different site types. For non-interacting spore systems, this dependence is always linear for all three site types as shown by the straight lines in Figure 4b. For the spore systems with excluded volume interaction, the average occupation numbers deviate from those of the non-interacting spore systems and this deviation increases with N . Note that as N increases, due to the excluded volume interaction, the $t=3$ sites lose their occupation number compared to those of non-interacting spore system, while the $t=2$ and $t=1$ sites gain some occupation.

In Figure 5, the validity of Equation 6 was checked for interacting spore systems by plotting the dependence of the two sides of this equation against each other using the attachment numbers of the site types

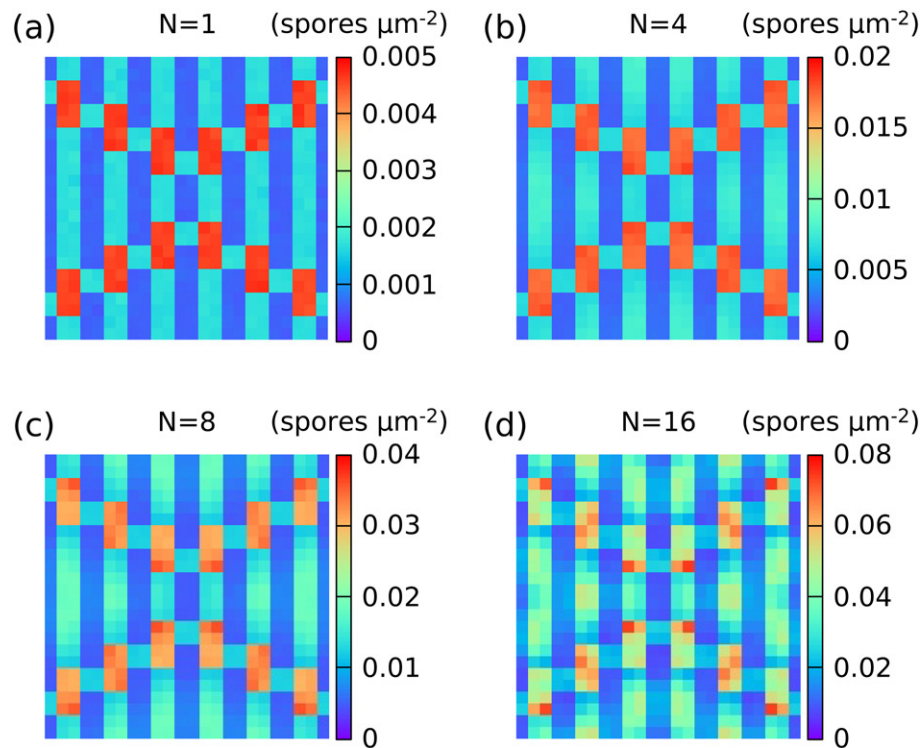


Figure 3. Attachment density maps for the systems considered in Figure 2 with $N=1$ (a), $N=4$ (b), $N=8$ (c) and $N=16$ (d) on a single unit cell. The attachment densities were obtained by calculating the average number of spores attached to each lattice site with Monte Carlo simulations. The density values given in units of spores μm^{-2} are indicated on the maps by colors.

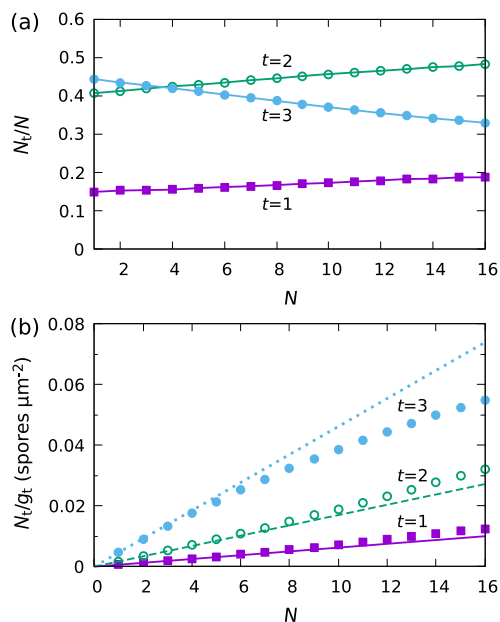


Figure 4. Dependence of the site-typed attachment probability (N_t/M) (a) and the average number of spores per lattice site (N_t/g_t) (b) for different site types t on the total number of spores (N). The data shown were obtained from the simulations of fouling on a single unit cell as shown in Figure 2 for spores with excluded volume interaction. The data points correspond to the site types of $t=1$ (filled circles), $t=2$ (open circles) and $t=3$ (squares). For comparison, the results for systems of non-interacting spores are shown in (b) as straight lines for $t=1$ (solid), $t=2$ (dashed) and $t=3$ (dotted).

and that of a smooth surface. Equation 6 is perfectly valid for systems of non-interacting spores, and is shown by a straight line in Figure 5 with the slope equal to 1. For spore systems with excluded volume interaction, as shown by the data points, a very good agreement with Equation 6 is seen for the systems with small numbers of spores of $N=1$ and $N=2$. For $N \geq 4$, the points deviated from the linear regression, with the deviation increasing with N . Interestingly, the experimental data compiled in Decker et al. (2013) also showed similar deviations from a linear regression predicted by the SEA model of non-interacting spores (see figure 11 in Decker et al. 2013).

The simulation results have shown that the effects of excluded volume increase with the total number of spores N , or equivalently the average spore density. The limiting cases of $N=1$ and $N=16$ considered in the simulations correspond to the average densities of 1,376 and 27,778 spores mm^{-2} , respectively. High settlement densities of up to 6,000 spores mm^{-2} have been reported for microtopographic surfaces fabricated from polydimethyl siloxane elastomer (PDME) (Callow et al. 2002). Thus, the excluded volume effect of spore–spore interaction ought to be present in those experimental observations, in which the average density reached thousands of spores mm^{-2} . On the other hand, the result also indicates that the excluded

volume effect can be safely neglected for systems in typical experiments where there is no clustering of spores and the average density is $< 1,000$ spores mm^{-2} .

Effects of spore–spore attraction

Next, the effect of spore–spore attraction on the attachment behaviors on topographic surfaces was

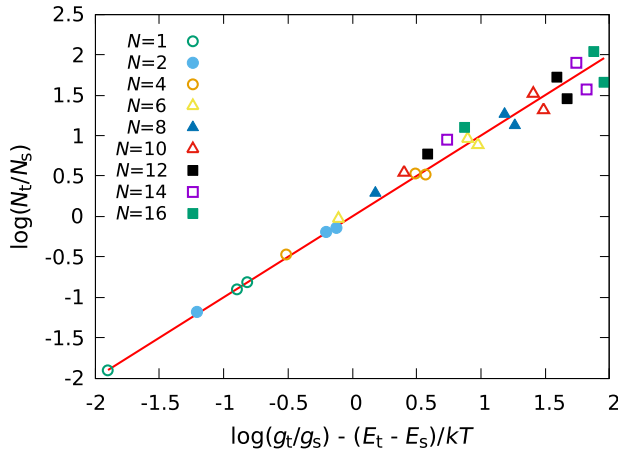


Figure 5. Comparison between the SEA model for non-interacting spores (solid line) and the SEA model with excluded volume interaction (data points). The solid line has a slope equal to 1 and corresponds to Equation 6. The data for the model of interacting spores were obtained from simulations on a single Sharklet unit cell with the number of spores N varied between 1 and 16 as indicated. It is assumed that the reference smooth surface has the number of attached spores $N_s = 1$.

studied. For this study, a system of $N=100$ spores was considered on a four-featured Sharklet surface of 4×4 unit cells, which corresponds to the average density of $10,851$ spores mm^{-2} . The same attachment energy parameters E_t were used as in the previous subsection. As described in the Methods section, the extended SEA model assigns an energy E_{int} for each pairwise contact between two nearby spores. A negative E_{int} promotes aggregation of spores. The simulations were carried out for various values of E_{int} between 0 and -4 kT . A strong aggregation tendency was observed for E_{int} lower than -2 kT . The top panels in Figure 6a–d show that the spores were fully and essentially dispersed at $E_{\text{int}} = 0$ and $E_{\text{int}} = -1$ kT , respectively, while strongly aggregated at $E_{\text{int}} = -2.2$ kT and $E_{\text{int}} = -3$ kT . For $E_{\text{int}} = -2.2$ kT , multiple aggregates may be observed at various sizes within a single configuration, whereas for $E_{\text{int}} = -3$ kT essentially a single large aggregate was established. In all cases, there are still non-aggregated spores due to thermal fluctuations.

In order to quantify the aggregation properties, following Decker et al. (2014), the radial distribution function (RDF) $g(r)$ of spores was calculated. The RDF is defined as the average number of spores found within a unit surface area located at a distance r to a given spore divided by the average density ρ of spores on the whole surface. The RDF can be considered as a relative probability of observing a spore at the distance r from a given spore. In the calculation,

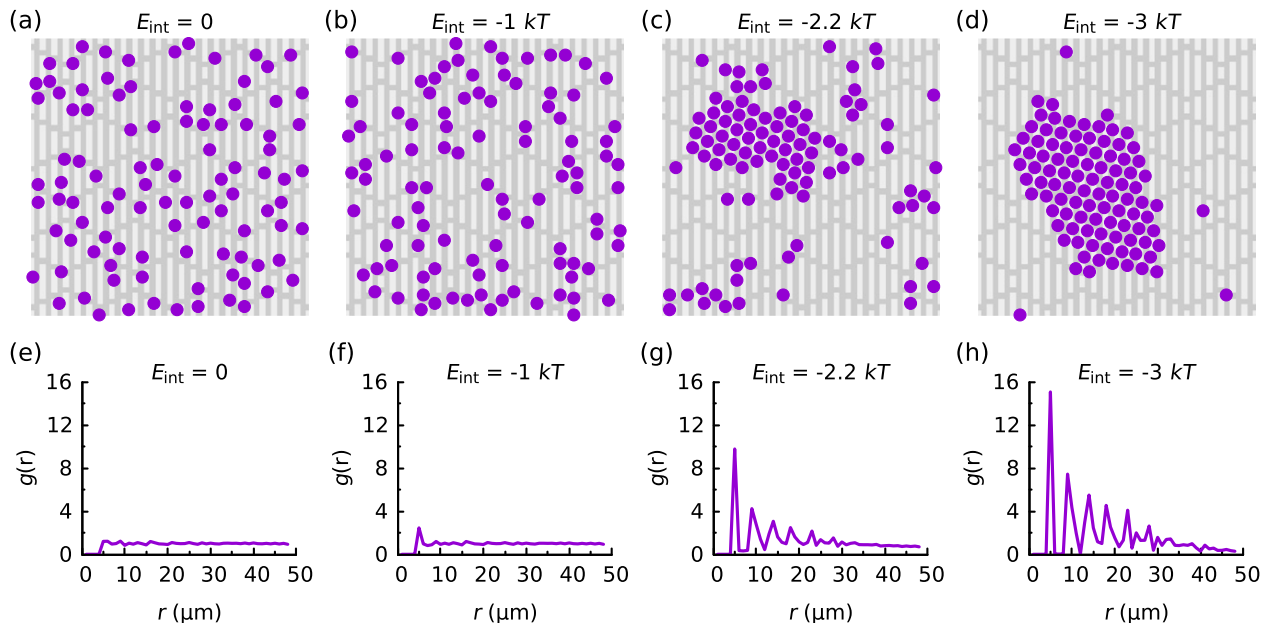


Figure 6. Examples of typical spore configurations on the lattice (top panels) and the radial distribution functions (bottom panels) for spore systems without spore–spore interaction (a, e) and with attractive spore–spore interactions (b–d, f–h). The results shown are obtained for systems of $N=100$ spores on the Sharklet surface of the size of 4×4 unit cells. The interaction energy parameter used in the simulations was $E_{\text{int}} = 0$ (a, e), $E_{\text{int}} = -1$ kT (b, f), $E_{\text{int}} = -2.2$ kT (c, g) and $E_{\text{int}} = -3$ kT (d, h).

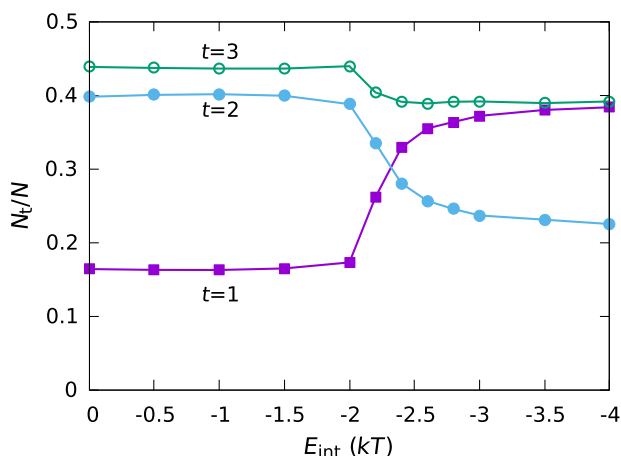


Figure 7. Dependence of site-typed attachment probability on the spore–spore interaction energy E_{int} for different site types t as indicated. The data are obtained for the systems of $N=100$ spores on the Sharklet surface of 4×4 unit cells as considered in Figure 6.

the function $g(r)$ was determined with a discretization of the distance r at $1 \mu\text{m}$ resolution and was obtained from the simulations by averaging over multiple spore configurations (the periodic boundary conditions were applied when counting the number of spores within a range of distance r). The plots of the RDF obtained for various values of interaction energy E_{int} are shown in Figure 6e–h. For $E_{\text{int}} = 0$ the function $g(r)$ is essentially flat and roughly equal to 1 (Figure 6e). The flat RDF corresponds to spore configurations without aggregates, such as the one shown in Figure 6a. For $E_{\text{int}} = -1 \text{ kT}$ the function $g(r)$ has only one small peak at short distance r (Figure 6f), indicating the formation of small aggregates. The cases of $E_{\text{int}} = -2.2 \text{ kT}$ (Figure 6g) and $E_{\text{int}} = -3 \text{ kT}$ (Figure 6h) show multiple peaks in the RDF and indicate the appearance of large aggregates. These indications are consistent with what was observed in the spore configurations shown in Figures 6b–d. The first peak in the RDF starting from small distances always occurs at r roughly equal to the spore diameter ($5 \mu\text{m}$), and the next peaks are separated by the distances of $4\text{--}5 \mu\text{m}$, indicating that spores in the aggregates are in contact with each other. It can be seen that as E_{int} decreases, more peaks and higher peaks of the RDF are observed, indicating that the average size of the aggregates increases with the strength of the attractive interaction.

Figure 7 shows the dependence of the site-typed attachment probabilities on the attraction energy E_{int} . For negative E_{int} larger than -2 kT , it is shown that these probabilities do not differ significantly from their values at $E_{\text{int}} = 0$. These probabilities undergo large changes for E_{int} between -2 kT and -3 kT . In

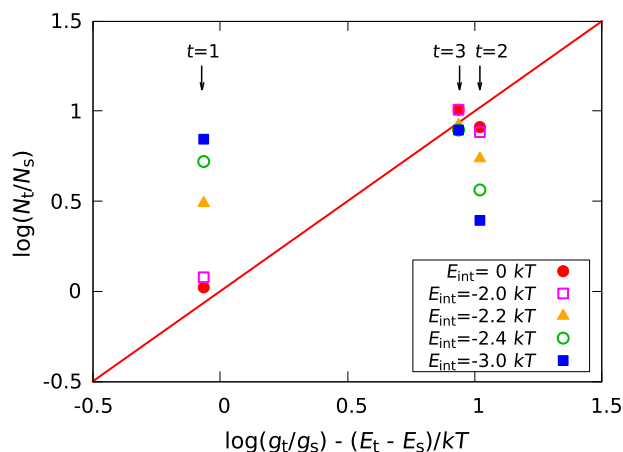


Figure 8. Comparison between the SEA model for non-interacting spores (solid line) and the SEA model with attractive interaction between spores (data points), for various values of interaction energy E_{int} and different site types t as indicated. The solid line has a slope equal to 1 and corresponds to Equation 6. The data for the model of interacting spores were obtained from the simulations of $N=100$ spores on the Sharklet surface of 4×4 unit cells as considered in Figure 6. For the present plot, the reference smooth surface is assumed to have $N_s = 16$ attached spores.

particular, the attachment probability for $t=1$ sites increased strongly with the magnitude of E_{int} while those of $t=2$ and $t=3$ sites decrease. For $E_{\text{int}} < -2.3 \text{ kT}$ there were more spores attached to the $t=1$ sites than to the $t=2$ sites, which is not the case for weaker attraction. Thus, sufficiently strong spore–spore attraction leads to a reshuffling of the preferential attachment order.

Figure 8 shows that the attractive interaction between spores leads to strong deviations in the attachment characteristics from those of the SEA model for non-interacting spores. The attachment numbers obtained in the model with attractive interaction are no longer consistent with Equation 6 for E_{int} lower than -2 kT , consistent with the spore clustering observed in the simulations. Note that the deviations from Equation 6 due to attractive interaction are much stronger than those induced by the excluded volume interaction shown in Figure 5. Figure 8 also shows that the deviations are much stronger for $t=1$ and $t=2$ sites than for the $t=3$ sites.

The appearance of multiple peaks in the RDF as well as the sharp changes in the site-typed attachment probabilities when E_{int} becomes lower than -2 kT indicate that the formation of clusters in biofouling is a kind of phase transition similar to the gas–liquid transition in two dimensions. Studies of the latter, eg for a 2-D Lennard–Jones fluid (Rovere et al. 1990), have shown that below a critical density this

transition is a first-order phase transition with observed phase coexistence and phase separation. One interesting observation from the simulation result is that the spores in the clusters are arranged in a honeycomb-like hexagonal packing (Figure 6), which is the densest packing of circles on a plane (Stephenson 2005). This packing arrangement has arisen naturally due to the spherical shape of the spores, but it is also interesting to note that it appeared on a topographic lattice which has no hexagonal symmetry. Here, due to a strong attractive spore–spore interaction, the mismatch between the lattice symmetry and the hexagonal symmetry was insufficient to destroy the optimal packing arrangement.

Decker et al. (2014) have recently shown that the zoospore *Ulva linza* forms aggregates when they attach to microtopographic surfaces, while the diatom *Navicula incerta* does not. These two types of organism showed similar behaviors to the spore models with and without attractive interaction considered in the present study. The present simulations indicate that there must be a significant attraction between the *U. linza* zoospores, of at least about $-2 kT$. This interaction energy may be obtained more precisely through a thorough comparison of experimental and simulation data. The study of Decker et al. (2014) also showed that surface topography and certain local attachment site geometries have measurable effects on the RDF of the aggregates of zoospores. The model proposed here would provide a useful tool for studying such effects.

Matching with experiment

Finally, an example is shown to illustrate how the SEA model can be tuned to match with an experiment and how the model can predict attachment behaviors for systems of increased number of spores and for a modified topographic surface. Consider the experiments reported by Long, Schumacher, et al. (2010) for *U. linza* zoospores, in which the spore attachments on both the four-featured Sharklet surface and the four-featured recessed Sharklet surface have been analyzed (the recessed surface has the features that are recessed). The experimental topographies have the same feature sizes and spacing as that shown in Figure 1. For the Sharklet surface, it was found that 96% of spores attached on the depressed regions ($t=2$ and $t=3$ sites), of which 56% attached on the intersection regions ($t=3$ sites). For the recessed Sharklet surface, 94% of the spores were reported to attach on the recessed regions. These statistics were obtained for individual spores that were not participating in the aggregates.

The attachment energy parameters for the SEA model were determined from the above experimental data for the Sharklet surface. These data yielded attachment probabilities $p_1 = 0.04$, $p_2 = 0.4$, and $p_3 = 0.56$ for the three site types. By using Equation 4, the energy differences for different pairs of site types were calculated. Because in the SEA model, only the energy differences, not their absolute values, determine the attachment probabilities, it was assumed that $E_1 = 0$ for the $t=1$ sites. The attachment energies obtained for the $t=2$ and $t=3$ sites are $E_2 = -2.303 kT$ and $E_3 = -3.555 kT$, respectively. These energies were used as inputs for the SEA model with the excluded volume interaction. Monte Carlo simulations were carried out in the latter model for multiple spore systems on both the Sharklet and the recessed Sharklet surfaces.

Figure 9 shows predictions of the site-typed attachment probabilities and the density maps obtained by the simulations for the four-featured Sharklet unit cell and the four-featured recessed Sharklet unit cell. In both cases, it is shown that due to the excluded volume effect, the attachment probability for $t=3$ sites decrease with the number of spores N while those for $t=1$ and $t=2$ sites increase. For the recessed Sharklet unit cell, the probability for the $t=3$ site type is always the highest among the three site types while for the Sharklet unit cell, this observation is true only for $N < 8$. This difference is due to the fact that the recessed Sharklet surface has more $t=3$ sites than the Sharklet one. For the $N=1$ case, the simulations showed that 93.4% of the spores attached to the recessed regions of the recessed Sharklet surface, which is very close to the experimental result of 94% (Long, Schumacher, et al. 2010). Figure 9 also shows that the spore density map changed completely when moving from the Sharklet surface to the recessed Sharklet one. For the former, the highest density corresponds to the intersection regions between features, whereas for the latter, the corners of the recessed features are the most strongly occupied by the spores.

Conclusions

Marine microorganisms attaching to a submerged surface may interact with each other through various mechanisms due to their excluded volume, the chemistry of their membrane's macromolecules, hydrophobicity, as well as the natural tendency of microorganisms to live as social communities. In this paper, an extended surface energetic attachment model was introduced for studying the fouling of interacting spores on topographic surfaces. It was shown that spore–spore interactions lead to

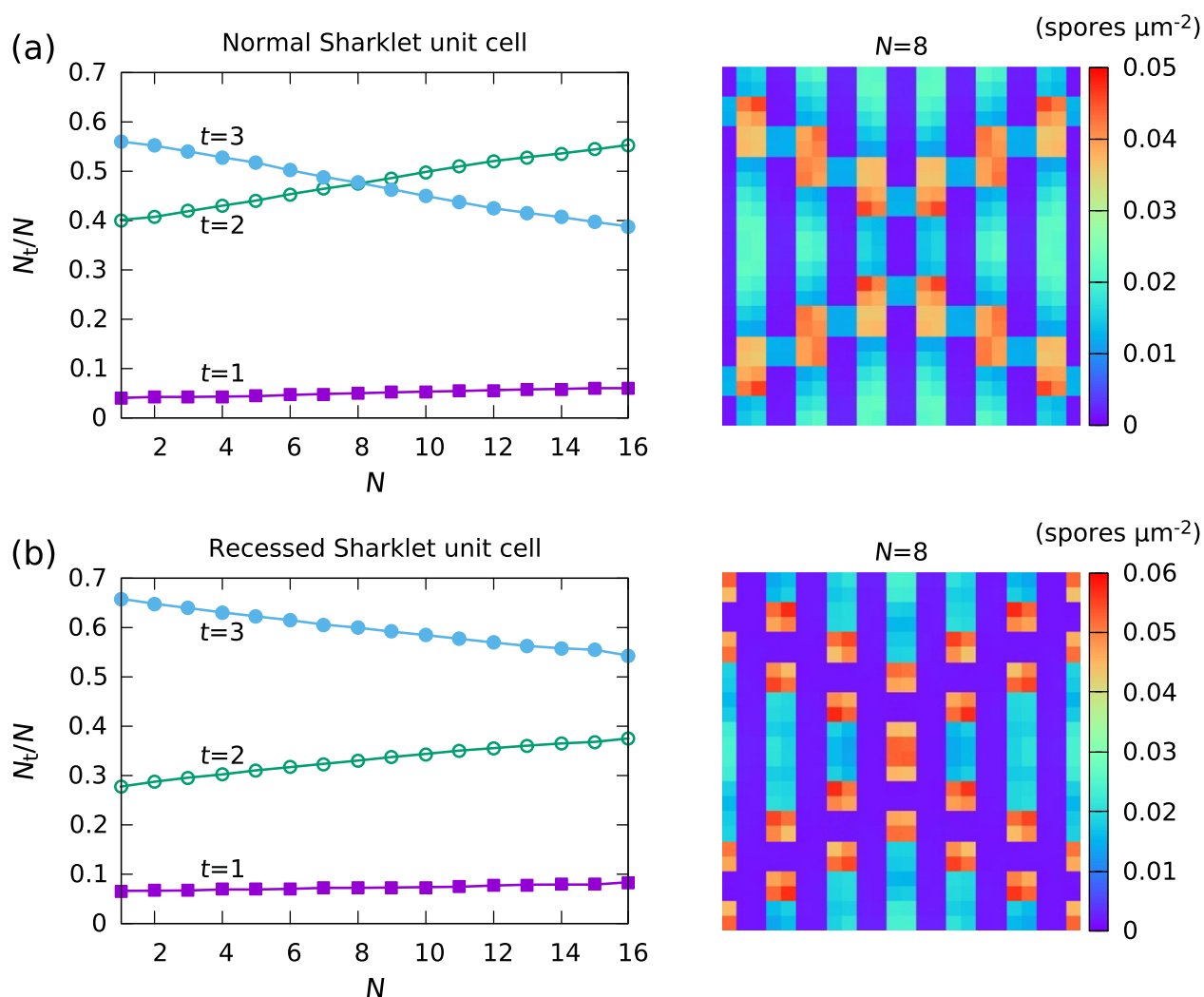


Figure 9. Prediction of spore attachment characteristics on the normal four-feathered Sharklet unit cell (a) and on the four-feathered recessed Sharklet unit cell (b) by using the SEA model with excluded volume interaction. The energy parameters of the model have been deduced from experimental data for the Sharklet surface (Long, Schumacher, et al. 2010). Left panels show the dependence of the site-typed attachment probability on the total number of spores N for different site types t as indicated. Right panels show the spore density maps for the case of $N=8$. The simulations were carried out on a single unit cell.

significant changes in the attachment behavior at high spore densities compared to those at low densities. Particularly, the excluded volume interaction lead to a relative decrease in attachment probability at the most favorable binding sites (eg the $t=3$ sites on the Sharklet topography) as the total number of spores on a surface is increased. The spore–spore attraction on the other hand lead to aggregation of attached spores. The average size of the aggregates increased with the strength of attraction. These behaviors can be easily verified by experiment or have been observed in the study of *U. linza* zoospores by Decker et al. (2014). The present study also demonstrated how the energy parameters of the model can be inferred from experimental data, allowing quantitative results to be obtained for real marine organisms. The model proposed here extends the predictive capability of the SEA model to high density

fouling and may serve as a powerful tool for the design of microtopographic AF surfaces.

Acknowledgements

One of the authors (TXH) acknowledges the support of Vietnam Academy of Science and Technology under the project named “Development of computational science research in specialized fields using high performance computers at VAST” (VAST.CTG.01/17-19).

Disclosure statement

The authors declare that they have no competing interests.

Funding

This work was supported by Office of Naval Research Global under grant number N62909-18-1-2009-P00001.

References

- Bloecher N, de Nys R, Poole AJ, Guenther J. 2013. The fouling hydroid *Ectopleura larynx*: a lack of effect of next generation antifouling technologies. *Biofouling*. 29: 237–246. doi:10.1080/08927014.2013.763228
- Callow ME, Jennings AR, Brennan AB, Seegert CE, Gibson A, Wilson L, Feinberg A, Baney R, Callow JA. 2002. Microtopographic cues for settlement of zoospores of the green fouling alga *Enteromorpha*. *Biofouling*. 18:229–236. doi:10.1080/08927010290014908
- Carman ML, Estes TG, Feinberg AW, Schumacher JF, Wilkerson W, Wilson LH, Callow ME, Callow JA, Brennan AB. 2006. Engineered antifouling microtopographies—correlating wettability with cell attachment. *Biofouling*. 22:11–21. doi:10.1080/08927010500484854
- Cassie AB, Baxter S. 1944. Wettability of porous surfaces. *Trans Faraday Soc.* 40:546–551. doi:10.1039/tf9444000546
- Decker JT, Kirschner CM, Long CJ, Finlay JA, Callow ME, Callow JA, Brennan AB. 2013. Engineered antifouling microtopographies: an energetic model that predicts cell attachment. *Langmuir*. 29:13023–13030. doi:10.1021/la402952u
- Decker JT, Sheats JT, Brennan AB. 2014. Engineered antifouling microtopographies: surface pattern effects on cell distribution. *Langmuir*. 30:15212–15218. doi:10.1021/la504215b
- Del Re B, Sgorbati B, Miglioli M, Palenzona D. 2000. Adhesion, autoaggregation and hydrophobicity of 13 strains of *Bifidobacterium longum*. *Letters in Applied Microbiology*. 31:438–442. doi:10.1046/j.1365-2672.2000.00845.x
- Efimenko K, Finlay J, Callow ME, Callow JA, Genzer J. 2009. Development and testing of hierarchically wrinkled coatings for marine antifouling. *ACS Appl Mater Interf.* 1:1031–1040. doi:10.1021/am9000562
- Katharios-Lanwermeier S, Xi C, Jakubovics NS, Rickard AH. 2014. Mini-review: microbial coaggregation: ubiquity and implications for biofilm development. *Biofouling*. 30: 1235–1251. doi:10.1080/08927014.2014.976206
- Kirschner CM, Brennan AB. 2012. Bio-inspired antifouling strategies. *Annu Rev Mater Res.* 42:211–229. doi:10.1146/annurev-matsci-070511-155012
- Long CJ, Finlay JA, Callow ME, Callow JA, Brennan AB. 2010. Engineered antifouling microtopographies: mapping preferential and inhibitory microenvironments for zoospore attachment. *Biofouling*. 26:941–952. doi:10.1080/08927014.2010.531390
- Long CJ, Schumacher JF, Robinson PA, Finlay JA, Callow ME, Callow JA, Brennan AB. 2010. A model that predicts the attachment behavior of *Ulva linza* zoospores on surface topography. *Biofouling*. 26:411–419. doi:10.1080/08927011003628849
- Magin CM, Cooper SP, Brennan AB. 2010. Non-toxic antifouling strategies. *Mater Today*. 13:36–44. doi:10.1016/S1369-7021(10)70058-4
- Magin CM, Long CJ, Cooper SP, Ista LK, López GP, Brennan AB. 2010. Engineered antifouling microtopographies: the role of Reynolds number in a model that predicts attachment of zoospores of *Ulva* and cells of *Cobetia marina*. *Biofouling*. 26:719–727. doi:10.1080/08927014.2010.511198
- Magin CM, Finlay JA, Clay G, Callow ME, Callow JA, Brennan AB. 2011. Antifouling performance of cross-linked hydrogels: refinement of an attachment model. *Biomacromolecules*. 12:915–922. doi:10.1021/bm101229v
- Marmur A. 2003. Wetting on hydrophobic rough surfaces: to be heterogeneous or not to be?. *Langmuir*. 19: 8343–8348. doi:10.1021/la0344682
- Metropolis N, Rosenbluth AW, Rosenbluth MN, Teller AH, Teller E. 1953. Equation of state calculations by fast computing machines. *J Chem Phys.* 21:1087–1092. doi:10.1063/1.1699114
- Reid B, Morris BM, Gow NA. 1995. Calcium-dependent, genus-specific, autoaggregation of zoospores of phytopathogenic fungi. *Experiment Mycol.* 19:202–213. doi:10.1006/emyc.1995.1025
- Rickard AH, McBain AJ, Stead AT, Gilbert P. 2004. Shear rate moderates community diversity in freshwater biofilms. *Appl Environ Microbiol.* 70:7426–7435. doi:10.1128/AEM.70.12.7426-7435.2004
- Savory AI, Grenville-Briggs LJ, Wawra S, van West P, Davidson FA. 2014. Auto-aggregation in zoospores of *Phytophthora infestans*: the cooperative roles of bioconvection and chemotaxis. *J R Soc Interface.* 11:20140017. doi:10.1098/rsif.2014.0017
- Scardino AJ, de Nys R. 2011. Mini review: biomimetic models and bioinspired surfaces for fouling control. *Biofouling*. 27:73–86. doi:10.1080/08927014.2010.536837
- Scardino AJ, Harvey E, De Nys R. 2006. Testing attachment point theory: diatom attachment on microtextured polyimide biomimics. *Biofouling*. 22:55–60. doi:10.1080/08927010500506094
- Scardino AJ, Guenther J, De Nys R. 2008. Attachment point theory revisited: the fouling response to a microtextured matrix. *Biofouling*. 24:45–53. doi:10.1080/08927010701784391
- Schembri MA, Kjaergaard K, Klemm P. 2003. Global gene expression in *Escherichia coli* biofilms. *Mol Microbiol.* 48:253–267. doi:10.1046/j.1365-2958.2003.03432.x
- Schumacher JF, Aldred N, Callow ME, Finlay JA, Callow JA, Clare AS, Brennan AB. 2007. Species-specific engineered antifouling topographies: correlations between the settlement of algal zoospores and barnacle cyprids. *Biofouling*. 23:307–317. doi:10.1080/08927010701393276
- Schumacher JF, Carman ML, Estes TG, Feinberg AW, Wilson LH, Callow ME, Callow JA, Finlay JA, Brennan AB. 2007. Engineered antifouling microtopographies—effect of feature size, geometry, and roughness on settlement of zoospores of the green alga *Ulva*. *Biofouling*. 23: 55–62. doi:10.1080/08927010601136957
- Rovere M, Heermann DW, Binder K. 1990. The gas-liquid transition of the two-dimensional Lennard-Jones fluid. *J Phys: Condens Matter.* 2:7009. doi:10.1088/0953-8984/2/33/013

- Stephenson K. 2005. Introduction to circle packing: the theory of discrete analytic functions. Cambridge, UK: Cambridge University Press.
- Thomas DD, Peterson AP. 1990. Chemotactic auto-aggregation in the water mould *Achlya*. *Microbiology*. 136:847–853.
- Thomas KV, Brooks S. 2010. The environmental fate and effects of antifouling paint biocides. *Biofouling*. 26:73–88. doi:10.1080/08927010903216564
- Wenzel RN. 1936. Resistance of solid surfaces to wetting by water. *Ind Eng Chem*. 28:988–994. doi:10.1021/ie50320a024
- Xiao L, Thompson S, Rohrig M, Callow ME, Callow JA, Grunze M, Rosenhahn A. 2013. Hot embossed microtopographic gradients reveal morphological cues that guide the settlement of zoospores. *Langmuir*. 29:1093–1099. doi:10.1021/la303832u